Study of Iterative Algorithms for Solving the Inverse Problem of Electrocardiography

Yujing Lin
Department of Electrical & Systems Engineering
School of Engineering & Applied Science
Email: yujing.lin@wustl.edu
Tel: (314)255-3793

Supervisor: R. Martin Arthur
Department of Electrical & Systems Engineering
School of Engineering & Applied Science
Email: rma@ese.wustl.edu
Tel: (314) 935-6167

Abstract

Changes in cardiac and torso geometry have both been investigated in their effects on the body-surface electrocardiograms (ECGs). Inverse solution of ECG mappings is widely used to get the cardiac electrophysiological information from the measured or simulated body-surface potentials (BSPs) so that heart-surface potentials (HSPs) can be reconstructed [2]. Because of the ill-postedness of the ECG inverse problem, regularization methods are usually used to obtain clinically reasonable solutions. In this project, we present two algorithms: the iterative least-mean-square method and the L1-norm-based iterative regularization technique in detail, and compare them with the traditional zero-order Tikhonov regularization scheme. Furthermore, we reconstruct the 3D models of HSPs and BSPs according to these three algorithms, and compare the spatial details of HSPs and BSPs that are generated from the different algorithms. Based on these algorithms which are applied to the inverse problems of ECG mappings, further studies regarding the spatial details of HSPs and BSPs, and the depolarization and repolarization of action potential templates on HSPs can be conducted, which will have a significant impact on the study of the identification of cardiac risks.

Keywords: inverse problem of ECG mappings; heart-surface potentials; body-surface potentials; zero-order Tikhonov regularization; iterative least-mean-square method; L1-norm-based iterative regularization; spatial details.

I. Introduction

Based on previous clinical research, we have known that the changes in both cardiac and torso geometry have effects on the body-surface electrocardiograms (ECGs). For example, the changes in cardiac geometry caused by type II diabetes mellitus (T2DM) will affect patients' body-surface ECGs (Fig.1). The standard 12-lead ECG set has been widely applied to identify cardiac risks [1]. This forward solution aims in diagnosing T2DM by identifying patients' habitus changes. However, as shown in Fig. 1, both diabetes and obesity may cause cardiac dysfunction, so either habitus changes with obesity or cardiac source changes with diabetes would affect patients' body-surface ECGs. Therefore, using the standard 12-lead analysis alone probably cannot provide enough spatial details for identifying the electrical phenotype of T2DM or some other cardiac-associated risks.

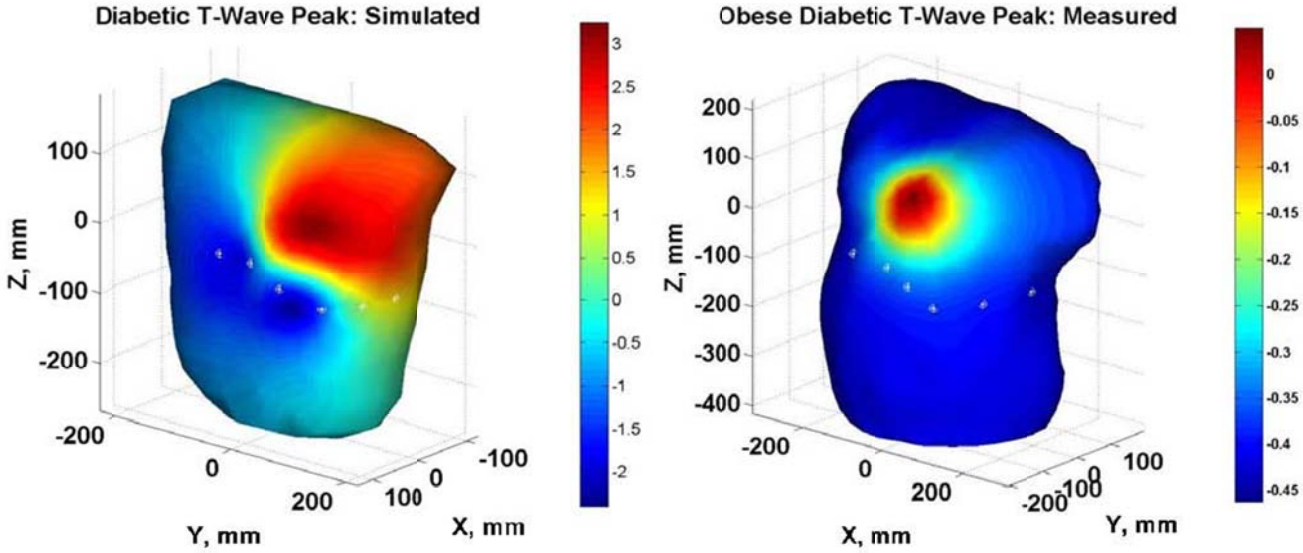

Fig.1. Anterior body-surface, iso-potential maps at the peak of T wave. (Left) Simulated map using body-surface potentials calculated from APs that combined all of the regional increases. (Right) Measured map in an obese diabetic subject. The white dots mark the locations of precordial electrodes in the standard 12-lead system [1].

In order to get more spatial information of patients' heart-surface potentials (HSPs), researchers are studying the inverse problem of ECG mapping. The inverse ECG solution is used to get the cardiac electrophysiological information from the measured or simulated body-surface potentials (BSPs) so that the HSPs can be reconstructed [2]. Because of the ill-postedness of the ECG inverse problems, regularization methods are used to obtain clinically reasonable solutions. Zero-order Tikhonov (ZOT) regularization is one common technique among the regularization schemes, which is often based on the L2-norm data and the corresponding constraint terms. However, even though L2-norm-based regularization methods can smooth the solution, the inverse solution provided by L2-norm-based methods is sensitive to measurement errors. Additionally, L2-norm-based methods cannot localize and distinguish

multiple proximal cardiac electrical sources [3]. Both of the above inadequacies of L2-norm-based regularization methods would affect the accuracy of simulation result significantly. Thus, total variation (TV) regularization method has been proposed to replace L2-norm-based regularization scheme in solving the inverse problems of ECG mappings.

The TV regularization method is a L1-norm-based technique, which can overcome the inadequacies of L2-norm-based regularization methods. Given the implementation of the L1-norm-based regularization method, we can not only remove the error caused by L2-norm-based regularization scheme, but also obtain more spatial information of cardiac electrical sources to reconstruct HSPs from measured or simulated BSPs.

In this project, we will not only present the iterative algorithm of L1-norm-based regularization scheme, but also come up with a completely different iterative algorithm which is derived by least-mean-square (LMS) method. Additionally, we will compare the reconstructions of HSPs that are generated from the L1-norm-based regularization method and the LMS algorithm with the HSPs generated from the ZOT regularization method. Moreover, we will apply these three different algorithms to reconstruct the corresponding BSPs so that we can compare the spatial details provided by the different HSPs and BSPs. Once proper algorithms can be developed to solve the inverse problems of ECG mappings, further clinical and bioelectrical research regarding different cardiac risks associated with HSPs and BSPs may be conducted, which will have a significant impact on the future study of cardiac diseases.

II. Iterative Algorithms for Solving the ECG Inverse Problems

In this section, we will present three different algorithms for solving the ECG inverse problems: the zero-order Tikhonov (ZOT) regularization method, the iterative least-mean-square (LMS) algorithm, and the L1-norm-based iterative regularization scheme. Furthermore, we will compare the similarities and differences among the reconstructions of the HSPs generated from these algorithms.

- **Zero-order Tikhonov Regularization Method**

ZOT regularization is a common regularization scheme, which is based on the L2-norm data and the corresponding constraints. Consider the following cost function [4]:

$$J_\tau(\boldsymbol{\Phi_H}) = \tau\|\boldsymbol{R\Phi_H}\|^2 + \|\boldsymbol{Z_{BH}\Phi_H} - \boldsymbol{\Phi_B}\|^2, \quad (1)$$

where $\boldsymbol{\Phi_H}$ and $\boldsymbol{\Phi_B}$ are HSPs and BSPs, respectively, τ is a regularization parameter, $\boldsymbol{Z_{BH}}$ is a transfer-coefficient matrix relating HSPs to BSPs, and $\boldsymbol{R}$ is a regularization matrix. Based on the previous research, we choose τ = 3.8983e-005. The notation $\|\cdot\|^2$ in the expression of $J_\tau(\boldsymbol{\Phi_H})$ represents L2-norm data, so the cost function $J_\tau(\boldsymbol{\Phi_H})$ can be rewritten as:

$$J_\tau(\boldsymbol{\Phi_H}) = \boldsymbol{\Phi_H^T}\left(\tau\boldsymbol{R^TR} + \boldsymbol{Z_{BH}^TZ_{BH}}\right)\boldsymbol{\Phi_H} - \boldsymbol{\Phi_H^TZ_{BH}^T\Phi_B} - \boldsymbol{\Phi_B^TZ_{BH}\Phi_H} + \boldsymbol{\Phi_B^T\Phi_B}. \quad (2)$$

The ZOT regularization method is based on minimizing $J_\tau(\boldsymbol{\Phi_H})$. Thus, taking the derivative of $J_\tau(\boldsymbol{\Phi_H})$ with respect to $\boldsymbol{\Phi_H}$ and setting the gradient function equal to $\mathbf{0}$ gives the estimate $\widehat{\boldsymbol{\Phi}}_{\boldsymbol{H}}$ that can minimize the cost function $J_\tau(\boldsymbol{\Phi_H})$:

$$\frac{\partial J_\tau(\boldsymbol{\Phi_H})}{\partial \boldsymbol{\Phi_H}} = 2\left(\tau \boldsymbol{R}^T \boldsymbol{R} + \boldsymbol{Z}_{\boldsymbol{BH}}^T \boldsymbol{Z}_{\boldsymbol{BH}}\right)\boldsymbol{\Phi_H} - 2\boldsymbol{Z}_{\boldsymbol{BH}}^T \boldsymbol{\Phi_B} = \mathbf{0}, \quad (3)$$

$$\widehat{\boldsymbol{\Phi}}_{\boldsymbol{H}} = \left(\tau \boldsymbol{R}^T \boldsymbol{R} + \boldsymbol{Z}_{\boldsymbol{BH}}^T \boldsymbol{Z}_{\boldsymbol{BH}}\right)^{-1} \boldsymbol{Z}_{\boldsymbol{BH}}^T \boldsymbol{\Phi_B}. \quad (4)$$

The regularization matrix $\boldsymbol{R}$ depends on the type of regularization technique. $\boldsymbol{R}$ could be either $\boldsymbol{I}$, the identity matrix; $\boldsymbol{L}$, the Laplacian operator; or $\boldsymbol{G}$, the gradient operator [4]. To analyze the ZOT regularization, we should choose $\boldsymbol{R} = \boldsymbol{I}$. The estimate $\widehat{\boldsymbol{\Phi}}_{\boldsymbol{H}}$ that can minimize the cost function $J_\tau(\boldsymbol{\Phi_H})$ is shown below.

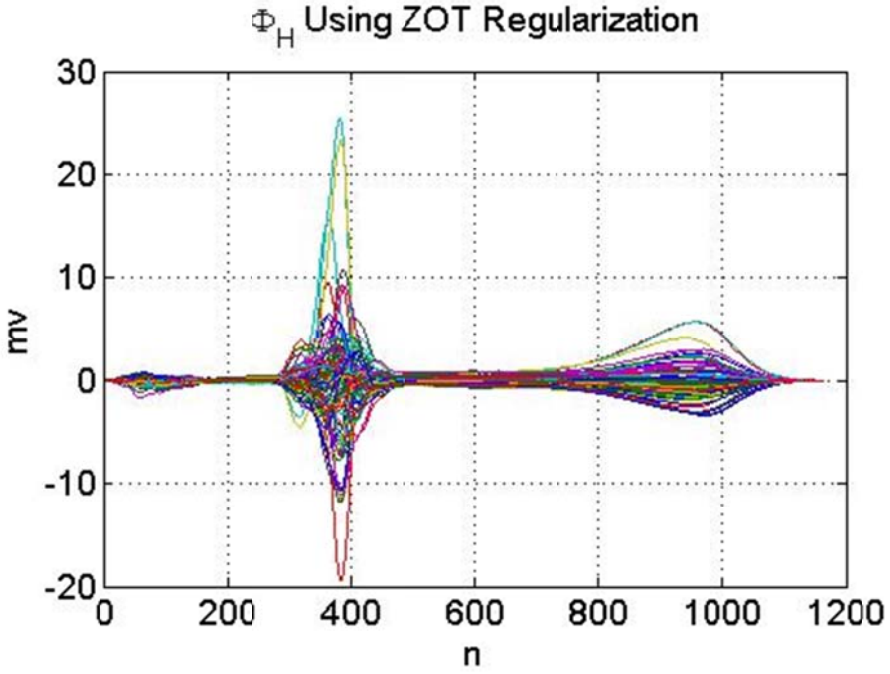

Fig.2: Estimate $\widehat{\boldsymbol{\Phi}}_{\boldsymbol{H}}$ generated by the ZOT regularization method.

- **Iterative Least Mean Square Algorithm**

The iterative LMS algorithm is an adaptive algorithm, which uses a gradient-based method of steepest descent. The general idea of the LMS algorithm is to use the estimates of the gradient vector from the available data. Meanwhile, it incorporates an iterative procedure that makes successive corrections to the weight vector, in the direction of the negative of the gradient vector, which eventually leads to the minimum mean-square error. Compared with other regularization algorithms, the LMS

algorithm is relatively simple because it does not require the calculations of correlation function and matrix inversions.

Before we apply the LMS algorithm to the inverse problem of ECG mappings, let us consider the following signal channel model [5]:

$$\boldsymbol{y} = \sum_{l=0}^{m-1} h[t-l]f[l] = \boldsymbol{h}^T\boldsymbol{f}, \quad (5)$$

where $\boldsymbol{h} = [h(t), h(t-1), \dots, h(t-m+1)]^T$, $\boldsymbol{f} = [f(0), f(1), \dots, f(m-1)]^T$.

Our objective is to find the estimate $\hat{\boldsymbol{f}}$ from the measurement $\boldsymbol{y}$ by minimize the following cost function:

$$J(\hat{\boldsymbol{f}}) = \left(\boldsymbol{y} - \boldsymbol{h}^T\hat{\boldsymbol{f}}\right)^2 = \boldsymbol{y}^T\boldsymbol{y} - \boldsymbol{y}^T\boldsymbol{h}^T\hat{\boldsymbol{f}} - \hat{\boldsymbol{f}}^T\boldsymbol{h}\boldsymbol{y} + \hat{\boldsymbol{f}}^T\boldsymbol{h}\boldsymbol{h}^T\hat{\boldsymbol{f}}, \quad (6)$$

which is the norm of the error between the measurement $\boldsymbol{y}$ and the estimate $\hat{\boldsymbol{y}} = \boldsymbol{h}^T\hat{\boldsymbol{f}}$.

To determine the estimate $\hat{\boldsymbol{f}}$ that can minimize $J(\hat{\boldsymbol{f}})$, take the derivative of $J(\hat{\boldsymbol{f}})$ with respect to $\hat{\boldsymbol{f}}$ so that we can get the gradient function:

$$\frac{\partial J(\hat{\boldsymbol{f}})}{\partial \hat{\boldsymbol{f}}} = -2\boldsymbol{h}\boldsymbol{y} + 2\boldsymbol{h}\boldsymbol{h}^T\hat{\boldsymbol{f}}. \quad (7)$$

Using gradient descent method to update $\hat{\boldsymbol{f}}$, we can obtain:

$$\begin{aligned}\hat{\boldsymbol{f}}[t+1] &= \hat{\boldsymbol{f}}[t] - \frac{1}{2}\varepsilon\frac{\partial J(\hat{\boldsymbol{f}}[t])}{\partial \hat{\boldsymbol{f}}[t]} \\ &= \hat{\boldsymbol{f}}[t] - \frac{1}{2}\varepsilon\left(-2\boldsymbol{h}\boldsymbol{y} + 2\boldsymbol{h}\boldsymbol{h}^T\hat{\boldsymbol{f}}\right) \\ &= \hat{\boldsymbol{f}}[t] + \varepsilon\left(\boldsymbol{h}\boldsymbol{y} - \boldsymbol{h}\boldsymbol{h}^T\hat{\boldsymbol{f}}[t]\right) \\ &= \hat{\boldsymbol{f}}[t] + \varepsilon\boldsymbol{h}\left(\boldsymbol{y} - \boldsymbol{h}^T\hat{\boldsymbol{f}}[t]\right), \quad (8)\end{aligned}$$

where the parameter ε should satisfy $0 < \varepsilon < \frac{2}{\max\left(eig(\boldsymbol{h}\boldsymbol{h}^T)\right)}$.

Now let us define $\boldsymbol{h} = \boldsymbol{Z_{BH}}^T$, $\hat{\boldsymbol{f}}^{(k)} = \hat{\boldsymbol{\Phi}}_{\boldsymbol{H}}^{(k)}$, $\boldsymbol{y} = \boldsymbol{\Phi_B}^T$, and apply the LMS algorithm (8) to the inverse problem of ECG mappings. We can get the following iterative solution:

$$\hat{\boldsymbol{\Phi}}_{\boldsymbol{H}}^{(k+1)} = \hat{\boldsymbol{\Phi}}_{\boldsymbol{H}}^{(k)} + \varepsilon\boldsymbol{Z_{BH}}^T\left(\boldsymbol{\Phi_B}^T - \boldsymbol{Z_{BH}}\hat{\boldsymbol{\Phi}}_{\boldsymbol{H}}^{(k)}\right), \quad (9)$$

where the superscript (k) and $(k+1)$ indicate the iteration numbers.

The iterative procedure depends on the initial value of $\hat{\boldsymbol{\Phi}}_{\boldsymbol{H}}^{(k)}$ and the parameter ε. To simplify the algorithm, we define the initial value $\boldsymbol{\Phi}_{\boldsymbol{H}}^{(0)} = \boldsymbol{0}$, and choose $\varepsilon = \frac{1}{\max(eig(\boldsymbol{R}))}$, where $\boldsymbol{R} = \boldsymbol{Z_{BH}}^T\boldsymbol{Z_{BH}}$.

Observe Eq. (9), the initial value $\boldsymbol{\Phi}_{\boldsymbol{H}}^{(0)} = \boldsymbol{0}$ will result in the maximum error between estimate BSPs

$\boldsymbol{Z_{BH}}\widehat{\boldsymbol{\Phi}}_{\boldsymbol{H}}^{(0)}$ and the measurement BSPs $\boldsymbol{\Phi_B}^T$; that is, $\boldsymbol{e}^{(0)} = \boldsymbol{e_{max}} = \boldsymbol{\Phi_B}^T - \boldsymbol{Z_{BH}}\widehat{\boldsymbol{\Phi}}_{\boldsymbol{H}}^{(0)} = \boldsymbol{\Phi_B}^T$. As $\widehat{\boldsymbol{\Phi}}_{\boldsymbol{H}}^{(k)}$ increases, the estimate BSPs $\boldsymbol{Z_{BH}}\widehat{\boldsymbol{\Phi}}_{\boldsymbol{H}}^{(k)}$ increases so that the corresponding error $\boldsymbol{e}^{(k)}$ decreases. Furthermore, if the iterative solutions generated by Eq. (9) are convergent, the error $\boldsymbol{e}^{(k)} = \boldsymbol{\Phi_B}^T - \boldsymbol{Z_{BH}}\widehat{\boldsymbol{\Phi}}_{\boldsymbol{H}}^{(k)}$ will eventually reach $\mathbf{0}$, which indicates that $\widehat{\boldsymbol{\Phi}}_{\boldsymbol{H}}^{(k+1)} = \widehat{\boldsymbol{\Phi}}_{\boldsymbol{H}}^{(k)}$ in that iteration.

Denote $\mu\big(\sigma(QRS)\big)^{(k)}$ as the notation standing for the mean of standard deviation of the QRS region of $\widehat{\boldsymbol{\Phi}}_{\boldsymbol{H}}^{(k)}$. We use the $\mu\big(\sigma(QRS)\big)^{(k)}$ to determine whether the solution $\widehat{\boldsymbol{\Phi}}_{\boldsymbol{H}}^{(k)}$ provided by Eq. (9) converges or not. When the estimate $\widehat{\boldsymbol{\Phi}}_{\boldsymbol{H}}^{(k)}$ updates, the changes of the HSPs in the QRS region are much more obvious than the changes in other regions. Therefore, the changes in the QRS region can be easily observed so that they are usually chosen to represent the overall changes in the estimate $\widehat{\boldsymbol{\Phi}}_{\boldsymbol{H}}^{(k)}$. To determine if $\widehat{\boldsymbol{\Phi}}_{\boldsymbol{H}}^{(k)}$ converges, we run 50000 iterations and generate the curve showing the changes of $\mu\big(\sigma(QRS)\big)^{(k)}$ as follows:

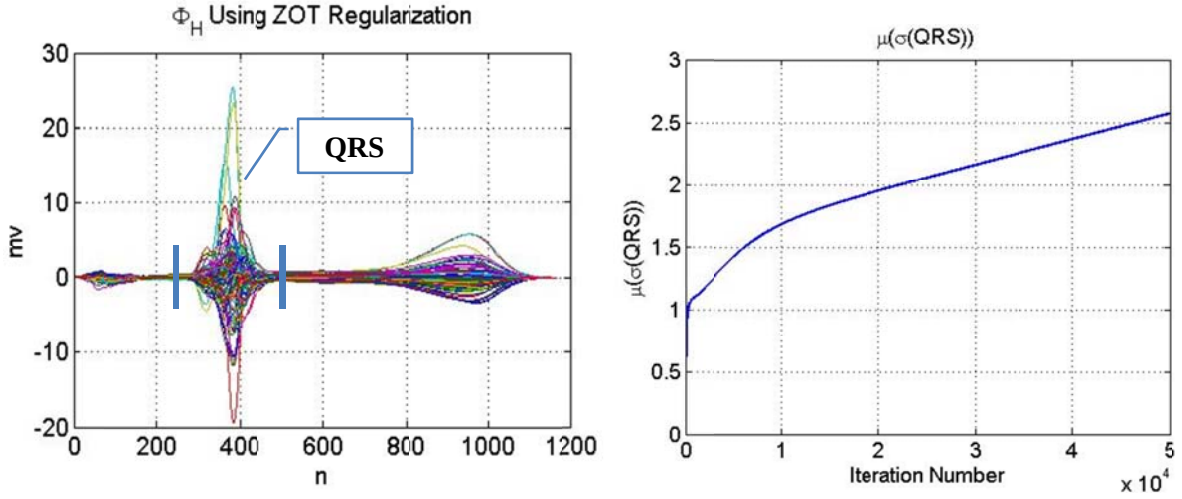

Fig.3: (Left) Estimate HSPs generated from the ZOT regularization; the region bounded by the two blue lines represents the QRS region. (Right) $\mu\big(\sigma(QRS)\big)$ generated for each iteration using the LMS algorithm.

From the right figure shown above, we see that the $\mu\big(\sigma(QRS)\big)^{(k)}$ keeps increasing within these 50000 iterations, which means that the estimate $\widehat{\boldsymbol{\Phi}}_{\boldsymbol{H}}^{(k)}$ does not converge in these 50000 iterations. We test more iteration, but the values of $\mu\big(\sigma(QRS)\big)^{(k)}$ still keep increasing. Therefore, we can conclude that using the iterative LMS algorithm, it is very difficult to find a convergent solution $\widehat{\boldsymbol{\Phi}}_{\boldsymbol{H}}^{(k)}$ in some amount of iterations.

Because it is hard to find a global minimum $\widehat{\boldsymbol{\Phi}}_{\boldsymbol{H}}^{(k)}$, we need to consider if we can determine a local minimum $\widehat{\boldsymbol{\Phi}}_{\boldsymbol{H}}^{(k)}$ in these 50000 iterations instead. We take the difference of $\mu\big(\sigma(QRS)\big)^{(k)}$ between

each two consecutive iterations; that is, $\mu\big(\sigma(QRS)\big)^{(k+1)} - \mu\big(\sigma(QRS)\big)^{(k)}$, to observe the increasing amount $\Delta\Big(\mu\big(\sigma(QRS)\big)\Big)$ between each two consecutive iterations.

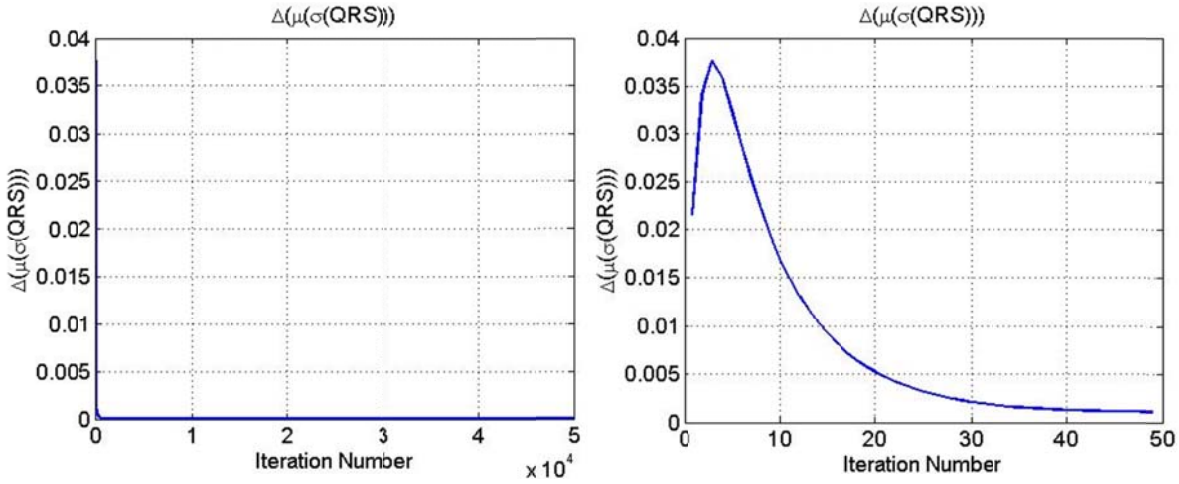

Fig. 4: $\Delta\Big(\mu\big(\sigma(QRS)\big)\Big)$ between each two consecutive iterations: (Left) 50000 iterations; (Right) 50 iterations.

From the left figure in Fig.4, we can find that the increasing amount $\Delta\Big(\mu\big(\sigma(QRS)\big)\Big)$ decreases to zero quickly when we run 50000 iterations, so it is very difficult to observe the $\Delta\Big(\mu\big(\sigma(QRS)\big)\Big)$ in the very beginning of these 50000 iterations clearly. Hence, we test 50 iterations instead to observe the $\Delta\Big(\mu\big(\sigma(QRS)\big)\Big)$ when k is small. From the right figure, we see that $\Delta\Big(\mu\big(\sigma(QRS)\big)\Big)$ increases quickly before the first three iterations, and then it starts to decrease after $k = 3$. Although $\Delta\Big(\mu\big(\sigma(QRS)\big)\Big)$ is decreasing after $k = 3$, $\mu\big(\sigma(QRS)\big)$ is still increasing as long as the value of $\Delta\Big(\mu\big(\sigma(QRS)\big)\Big)$ is positive.

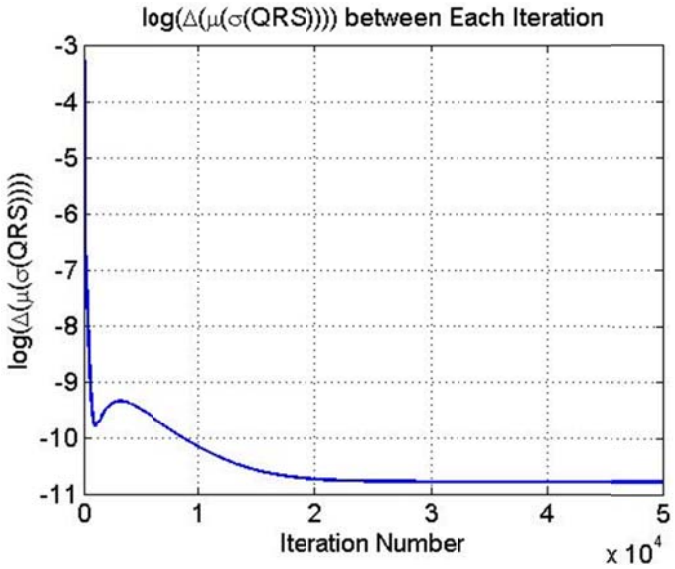

Fig. 5: $\log\Delta\Big(\mu\big(\sigma(QRS)\big)\Big)$ between each two consecutive iterations using the LMS algorithm.

To observe the change of $\mu(\sigma(QRS))$ clearly, we took the logarithm of $\Delta\left(\mu(\sigma(QRS))\right)$, and plot the value of $\log\Delta\left(\mu(\sigma(QRS))\right)$ (Fig. 5). From Fig. 5, we see that after $k \approx 3000$, $\log\Delta\left(\mu(\sigma(QRS))\right)$ keeps decreasing, and then it starts to increase around $k = 48000$. Thus, we may assume there exists a local minimum point between $k = 3000$ and 48000, which means that we can find the location of the minimum $\log\Delta\left(\mu(\sigma(QRS))\right)$ to determine the stop iteration. We can find that the minimum value of $\log\Delta\left(\mu(\sigma(QRS))\right)$ appears at $k = 37189$ by using Matlab. Additionally, we need to pay attention to the parameter ε, because it can affect the increasing rate of $\mu(\sigma(QRS))$. Recall Eq. (9), the value of ε affects the increasing amount for $\widehat{\boldsymbol{\Phi}}_{\boldsymbol{H}}^{(k)}$ in each iteration. The larger ε is, the less iteration we need to reach the local minimum point. However, if ε becomes too large, the curve of $\Delta\left(\mu(\sigma(QRS))\right)^{(k)}$ will oscillate, that is why there exists an upper bound for the choice of ε. In this study, we choose the parameter $\varepsilon = \frac{1}{\max(eig(\boldsymbol{R}))} = 0.6379$.

We generate 37189 iterations, and then compare the estimate $\widehat{\boldsymbol{\Phi}}_{\boldsymbol{H}}^{(37189)}$ with the $\widehat{\boldsymbol{\Phi}}_{\boldsymbol{H}}$ generated from the ZOT regularization technique.

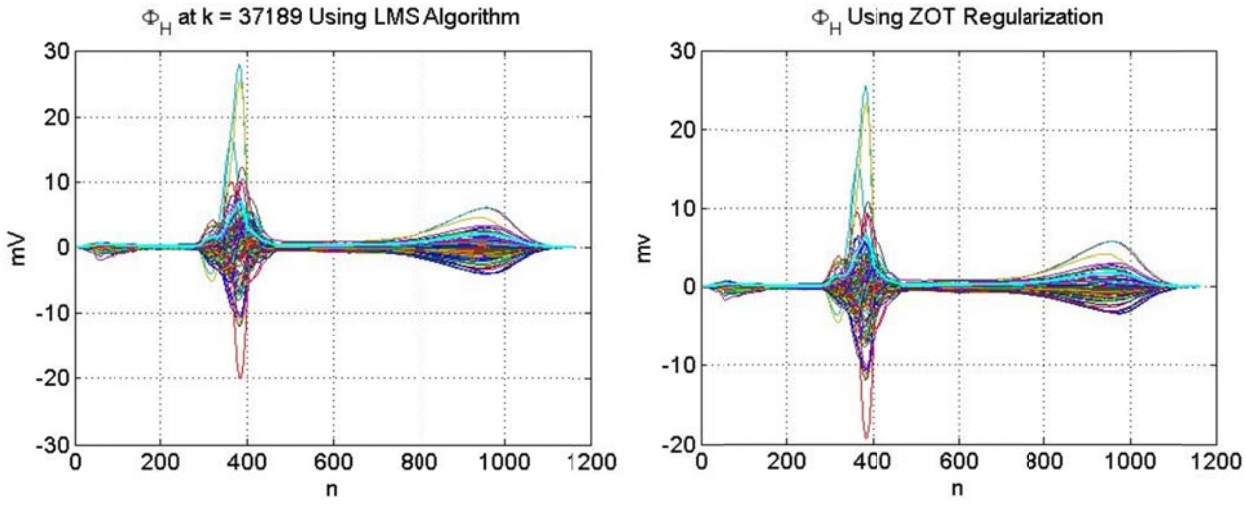

Fig. 6: (Left) Estimate $\widehat{\boldsymbol{\Phi}}_{\boldsymbol{H}}^{(37189)}$ generated from the LMS algorithm. (Right) Estimate $\widehat{\boldsymbol{\Phi}}_{\boldsymbol{H}}$ generated from the ZOT regularization. The cyan lines in both of the figures indicate the standard deviation at each node.

From the overall shape and the magnitude value of the HSPs shown in Fig. 6, we see that the estimate $\widehat{\boldsymbol{\Phi}}_{\boldsymbol{H}}$ generated from the iterative LMS algorithm and the ZOT regularization method are very close to each other. Calculating the relative error (RE) and the correlation coefficient (CC) between these two estimate HSPs gives: RE = 0.1874 and CC = 0.9884. This result shows that the iterative LMS algorithm is a good approximation to the ZOT regularization method, and it can generate very close $\widehat{\boldsymbol{\Phi}}_{\boldsymbol{H}}$

without considering L2-norm data and the corresponding constraints, so the LMS algorithm can overcome the inadequacies of the ZOT regularization technique. The only disadvantage of the LMS algorithm is that it usually needs more than 30000 iterations to obtain a good estimate solution $\widehat{\boldsymbol{\Phi}}_{\boldsymbol{H}}$, which takes too much testing time. In the next part, we are going to introduce another iterative regularization algorithm.

- **L1-Norm-Based Iterative Regularization Scheme**

The ZOT regularization is a very common L2-norm-based technique; however, although the L2-norm-based algorithms can smooth the solutions, they may reduce the accuracy of localizing cardiac sources. Additionally, they may affect the accuracy of resolving multiple sources in close proximity [2]. Since the total-variation (TV) regularization, which is also known as non-quadratic regularization method, has been widely used in the image restoration, there also exists a development of L1-norm-based approaches for magnetoencephalography (MEG) and electroencephalography (EEG). The L1-norm-based technique has been established as superior to higher order norms. This technique penalizes the L1-norm of the gradient function and yields less-smoothed solutions with more localized details. Hence, we are going to apply a L1-norm-based regularization scheme here, which bases on the L1-norm of the normal derivative of the HSPs. The cost function in Eq. (1) can be modified as:

$$J_{\lambda}(\boldsymbol{\Phi}_{\boldsymbol{H}}) = \lambda \left\| \frac{\partial \boldsymbol{\Phi}_{\boldsymbol{H}}}{\partial \boldsymbol{n}} \right\|_1^{\,2} + \|\boldsymbol{Z}_{\boldsymbol{BH}}\boldsymbol{\Phi}_{\boldsymbol{H}} - \boldsymbol{\Phi}_{\mathbf{B}}\|_2^{\,2}, \quad (10)$$

where λ is the L1-norm-based regularization parameter, the subscripts 1 and 2 indicate L1 norm and L2 norm, respectively. Define a normal derivative matrix $\boldsymbol{D}$, which can be derived to relate $\frac{\partial \boldsymbol{\Phi}_{\boldsymbol{H}}}{\partial \boldsymbol{n}}$ to $\boldsymbol{\Phi}_{\boldsymbol{H}}$:

$$\frac{\partial \boldsymbol{\Phi}_{\boldsymbol{H}}}{\partial \boldsymbol{n}} = \boldsymbol{D}\boldsymbol{\Phi}_{\boldsymbol{H}}. \quad (11)$$

Then, the cost function can be expressed as:

$$J_{\lambda}(\boldsymbol{\Phi}_{\boldsymbol{H}}) = \lambda\|\boldsymbol{D}\boldsymbol{\Phi}_{\boldsymbol{H}}\|_1^{\,2} + \|\boldsymbol{Z}_{\boldsymbol{BH}}\boldsymbol{\Phi}_{\boldsymbol{H}} - \boldsymbol{\Phi}_{\mathbf{B}}\|_2^{\,2}. \quad (12)$$

To minimize the cost function shown in (12), the most important task is to identify the normal derivative operator $\boldsymbol{D}$. This operator $\boldsymbol{D}$ can be derived from the geometric relationship between the HSPs and the BSPs [6]:

$$\boldsymbol{D} = -\boldsymbol{G}_{\boldsymbol{HH}}^{\,-1}\boldsymbol{P}_{\boldsymbol{HH}}, \quad (13)$$

where $\boldsymbol{P}_{\boldsymbol{HH}}$ represents the angles on heart surface, and $\boldsymbol{G}_{\boldsymbol{HH}}$ is the gradient of HSPs on heart surface.

Eq. (12) shows a nonlinear optimization problem. Due to non-differentiability of the L1-norm penalty function, an estimated solution can be obtained by [8]:

$$\widehat{\boldsymbol{\Phi}}_{\boldsymbol{H}} = \left(\boldsymbol{Z}_{\boldsymbol{BH}}^{\boldsymbol{T}}\boldsymbol{Z}_{\boldsymbol{BH}} + \lambda\boldsymbol{D}^{\boldsymbol{T}}\boldsymbol{W}_{\boldsymbol{\beta}}(\widehat{\boldsymbol{\Phi}}_{\boldsymbol{H}})\boldsymbol{D}\right)^{-1}\boldsymbol{Z}_{\boldsymbol{BH}}^{\boldsymbol{T}}\boldsymbol{\Phi}_{\boldsymbol{B}}, \quad (14)$$

where $\boldsymbol{W_\beta}(\widehat{\boldsymbol{\Phi}}_{\boldsymbol{H}})$ is the weight matrix of $\widehat{\boldsymbol{\Phi}}_{\boldsymbol{H}}$, and $\boldsymbol{D}$ is equal to the normal derivative operator shown in Eq. (13). The diagonal weight matrix $\boldsymbol{W_\beta}(\widehat{\boldsymbol{\Phi}}_{\boldsymbol{H}})$ is obtained by:

$$\boldsymbol{W_\beta}\left(\widehat{\boldsymbol{\Phi}}_{\boldsymbol{H}}\right) = \frac{1}{2} diag\left[\frac{1}{\sqrt{\left\|\boldsymbol{D}\widehat{\boldsymbol{\Phi}}_{\boldsymbol{H}}\right\|_1^2 + \beta}}\right], \quad (15)$$

where β is a small positive number, which can guarantee that the denominator of each element in the $\boldsymbol{W_\beta}\left(\widehat{\boldsymbol{\Phi}}_{\boldsymbol{H}}\right)$ is nonzero. In our problem, we choose $\beta = 10^{-5}$.

Consider L1-norm of a matrix **A**:

$$\|\boldsymbol{A}\|_1 = \max_{1\le j\le n} \sum_{j=1}^{m} |a_{ij}|, \quad (16)$$

which is simply the maximum absolute column sum of the matrix. Substituting $\boldsymbol{A} = \boldsymbol{D\Phi_H}$ yields:

$$\left\|\boldsymbol{D}\widehat{\boldsymbol{\Phi}}_{\boldsymbol{H}}\right\|_1 = \max_{1\le j\le n} \sum_{j=1}^{m} |\phi'_{H_{ij}}|, \quad (17)$$

$$\phi'_{H_{ij}} = \text{element locating in } i_{th} \text{ row and } j_{th} \text{ column of } \boldsymbol{D}\widehat{\boldsymbol{\Phi}}_{\boldsymbol{H}}.$$

As what we have mentioned in the introduction, regularization algorithms for the inverse ECG mapping problems are often used to generate clinically reasonable solutions to ill-posed problems. For the ZOT regularization method, the regularization parameter τ has been solved under previous related research, but the L1-norm-based regularization parameter λ is unknown. Thus, before we further formularize the L1-norm-based iterative regularization algorithm, we first need to solve an appropriate regularization parameter λ.

L-curve is a parametric plot of the size of regularized solution and the corresponding residual [10]. We know that a good method for choosing the regularization parameter for discrete ill-posed problems is to incorporate information about the solution size in addition to using information about the residual size. The corner of the L-curve corresponds to a good balance between minimization of the sizes, and the corresponding regularization parameter λ is a good one.

The L1-norm-based L-curve shown below reveals the relationship between the L1-norm of the estimate HSPs and the residuals of the corresponding BSPs (BSPR). Each red dot in the plot represents a pair of $\left(\text{BSPR}, \left|\frac{\partial\widehat{\boldsymbol{\Phi}}_{\boldsymbol{H}}}{\partial \boldsymbol{n}}\right|\right)$, and the blue asterisk represents the corner of the L-curve in our case, where it corresponds to a good balance between minimization of the sizes. The corresponding regularization value is 0.1836. Thus, we choose $\lambda = 0.1836$ as our L1-norm-based regularization parameter.

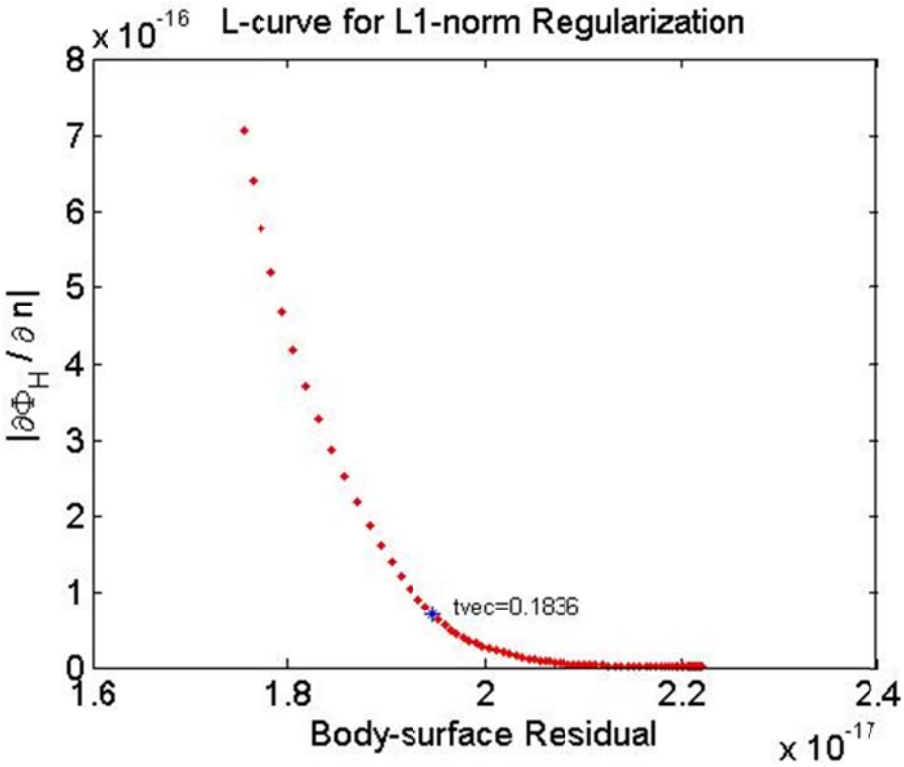

Fig. 7: L-curve for the L1-norm-based regularization scheme. The value of tvec at the blue asterisk is the L1-norm-based regularization parameter λ.

Once we obtain the regularization parameter λ, we can formularize the L1-norm-based iterative algorithm as follows:

Initialization:

$$\widehat{\boldsymbol{\Phi}}_{\boldsymbol{H}}^{(0)} = \left(\boldsymbol{Z}_{\boldsymbol{BH}}^{\boldsymbol{T}}\boldsymbol{Z}_{\boldsymbol{BH}} + \lambda \boldsymbol{D}^{\boldsymbol{T}}\boldsymbol{D}\right)^{-1}\boldsymbol{Z}_{\boldsymbol{BH}}^{\boldsymbol{T}}\boldsymbol{\Phi}_{\boldsymbol{B}}, \quad (18)$$

For step $k = 1,2, \ldots$

$$\boldsymbol{W}_{\boldsymbol{\beta}}^{(k)}\left(\widehat{\boldsymbol{\Phi}}_{\boldsymbol{H}}^{(k-1)}\right) = \frac{1}{2}diag\left[\frac{1}{\sqrt{\left|\left[\boldsymbol{D}\widehat{\boldsymbol{\Phi}}_{\boldsymbol{H}}^{(k-1)}\right]_1\right|^2 + \beta}}\right], \quad (19)$$

$$\widehat{\boldsymbol{\Phi}}_{\boldsymbol{H}}^{(k)} = \left(\boldsymbol{Z}_{\boldsymbol{BH}}^{\boldsymbol{T}}\boldsymbol{Z}_{\boldsymbol{BH}} + \lambda \boldsymbol{D}^{\boldsymbol{T}}\boldsymbol{W}_{\boldsymbol{\beta}}^{(k)}\left(\boldsymbol{\Phi}_{\mathbf{H}}^{(k-1)}\right)\boldsymbol{D}\right)^{-1}\boldsymbol{Z}_{\boldsymbol{BH}}^{\boldsymbol{T}}\boldsymbol{\Phi}_{\boldsymbol{B}}, \quad (20)$$

$$\boldsymbol{D} = -\boldsymbol{G}_{\boldsymbol{HH}}{}^{-1}\boldsymbol{P}_{\boldsymbol{HH}}, \quad (21)$$

$$\lambda = 0.1836, \quad (22)$$

$$\beta = 10^{-5}. \quad (23)$$

Similar to the LMS iterative algorithm, we use the $\mu\left(\sigma(QRS)\right)^{(k)}$ as the criterion to determine the stop iteration.

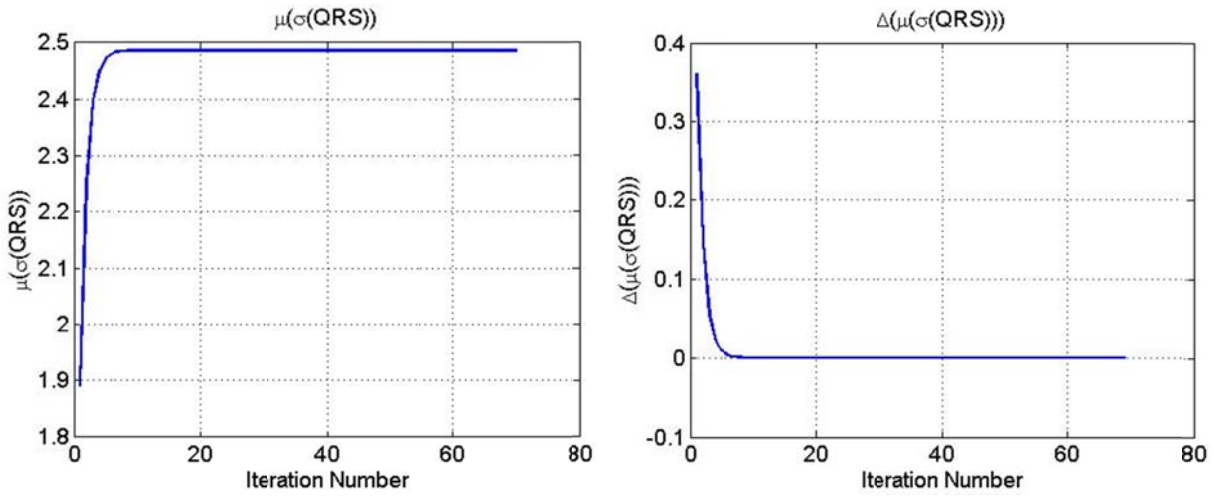

Fig. 8: (Left) $\mu(\sigma(QRS))$ for each iteration using the L1-norm-based iterative regularization. (Right) $\Delta\left(\mu(\sigma(QRS))\right)$ between each two consecutive iterations.

We can see that the $\mu(\sigma(QRS))$ of estimate HSPs generated from the L1-norm-based iterative regularization increases very fast at the beginning, and the difference of $\mu(\sigma(QRS))$ between each two consecutive iterations almost reaches zero within 10 iterations. To obverse the change of $\Delta\left(\mu(\sigma(QRS))\right)$ more clearly, we plot the corresponding $\log\Delta\left(\mu(\sigma(QRS))\right)$ as follows:

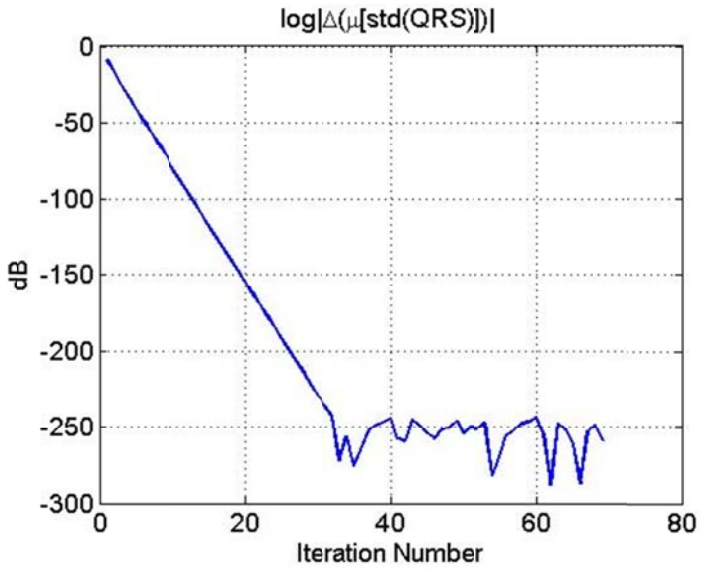

Fig. 9: $\log\Delta\left(\mu(\sigma(QRS))\right)$ between each two consecutive iterations using the L1-norm-based iterative regularization.

From Fig. 9, we notice that the $\log\left|\Delta\left(\mu(\sigma(QRS))\right)\right|$ keeps decreasing smoothly when k ranges from 0 to 33. After $k = 33$, the difference begins to oscillate, which means that the iteration number cannot go beyond 33 if we want to locate the local minimum point.

The $\mu(\sigma(QRS))$ decreases very fast within the 33 iterations, for example, when $k = 10$, $\Delta\left(\mu(\sigma(QRS))\right)^{(10)} = -80dB$, and when k increases to 20, $\left(\mu(\sigma(QRS))\right)^{(20)}$ decreases to $-150dB$. If we define $\Delta\mu(\sigma(QRS))^{(k)} = -100dB$ as the criterion to determine the stop iteration, we can stop at $k = 13$, and the relative error and correlation coefficient between $\widehat{\boldsymbol{\Phi}}_{\boldsymbol{H}}^{(13)}$ and the $\widehat{\boldsymbol{\Phi}}_{\boldsymbol{H}}$ generated from the ZOT regularization method are RE = 0.3131 and CC = 0.9525, respectively. An interesting result is that when k increases from 13 to 32, even though the $\Delta\mu(\sigma(QRS))$ decreases from $-100dB$ to $-250dB$, the relative error and correlation do not change. Hence, we can say the estimate $\widehat{\boldsymbol{\Phi}}_{\boldsymbol{H}}^{(k)}$ almost maintains consistent within a specific range of iterations.

To further explicitly show the difference of $\widehat{\boldsymbol{\Phi}}_{\boldsymbol{H}}^{(k)}$ in each iteration, and to determine the range of iterations, within which the estimate $\widehat{\boldsymbol{\Phi}}_{\boldsymbol{H}}^{(k)}$ maintains consistent, we generate a table to record the relative error and correlation coefficient between the $\widehat{\boldsymbol{\Phi}}_{\boldsymbol{H}}^{(k)}$ generated from the L1-norm-based iterative regularization and the $\widehat{\boldsymbol{\Phi}}_{\boldsymbol{H}}$ generated from the ZOT regularization.

Iteration Number	Relative Error (RE)	Correlation Coefficient (CC)
1	0.4359	0.9096
2	0.3218	0.9470
3	0.3093	0.9517
4	0.3106	0.9524
5	0.3119	0.9525
6	0.3126	0.9525
7	0.3129	0.9525
8-9	0.3130	0.9525
10-33	0.3131	0.9525

Table 1: Relative error and correlation coefficient of $\widehat{\boldsymbol{\Phi}}_{\boldsymbol{H}}^{(k)}$ generated from the L1-norm regularization and $\widehat{\boldsymbol{\Phi}}_{\boldsymbol{H}}$ generated from the ZOT regularization. The red-marked 0.9525 shown in the CC column show that CC doesn't change after the fifth iteration.

Recall that if we use the iterative LMS algorithm, we need more than 30000 iterations to get RE = 0.1874 and CC = 0.9884. However, only one iteration can result in RE = 0.4359 and CC = 0.9096 if we apply the iterative L1-norm-based regularization method. Moreover, when utilizing the iterative L1-norm-based regularization method, the CC starts to maintain at 0.9525 from the 5th iteration. Additionally, from 10th iteration, neither the relative error nor the correlation coefficient change. These features of the results have the following significant meanings.

We have shown that the LMS algorithm is a good approximation to the ZOT regularization, and the idea of the LMS algorithm is very straightforward. However, it usually takes thousands of iterations to reach our expected HSPs. As another iterative algorithm, the L1-norm-based regularization method only needs $\frac{1}{3000}$ of the time that the LMS method would use, so applying L1-norm-based algorithm can save a large amount of testing time. But compared with LMS algorithm, the RE generated by L1-norm-based algorithm is much larger, even though the CC is high. This means that the spatial details of the estimate HSPs generated from the iterative L1-norm-based regularization are different from the spatial details of the HSPs obtained by the iterative LMS algorithm or the ZOT method. Thus, to further compare and discuss these algorithms, we may need to study the reconstructions of corresponding BSPs.

From Table 1, we know $\widehat{\boldsymbol{\Phi}}_{\boldsymbol{H}}^{(k)}$ almost maintains consistent from k = 10, and if we pick k = 30, the comparison between $\widehat{\boldsymbol{\Phi}}_{\boldsymbol{H}}^{(30)}$ and the $\widehat{\boldsymbol{\Phi}}_{\boldsymbol{H}}$ generated from the ZOT regularization is shown below:

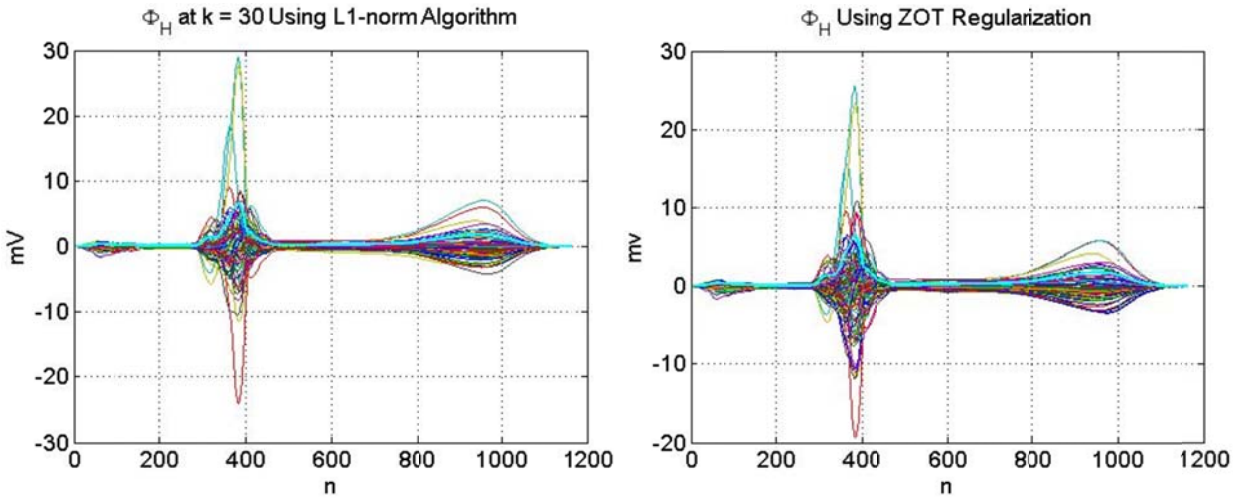

Fig. 10: (Left) Estimate $\widehat{\boldsymbol{\Phi}}_{\boldsymbol{H}}$ generated from the L1-norm iterative regularization. (Right) Reconstructed $\widehat{\boldsymbol{\Phi}}_{\boldsymbol{H}}$ generated from the ZOT regularization. The cyan lines indicate the standard deviation at each node.

A brief table given below is to summarize the differences between the LMS iterative algorithm and the L1-norm-based regularization method. From the data, we can clearly see that compared with the L1-norm-based regularization method, the LMS algorithm is more approximate to ZOT regularization, but it takes much more iterations to generate the expected HSPs.

	Stop Iteration	Relative Error	Correlation Coefficient	Regularization Parameter
LMS Algorithm	**37189**	**0.1874**	**0.9884**	**3.8983e-005**
L1 Algorithm	**10**	**0.3131**	**0.9525**	**0.1836**

Table 2: Comparison between the LMS iterative algorithm and the L1-norm-based regularization method. The relative error and correlation coefficient are compared with ZOT regularization method.

III. Reconstructions of Body-Surface Potentials

Before we compare the calculated BSPs generated from different iterative algorithms, let us further compare the estimate $\hat{\boldsymbol{\Phi}}_{\boldsymbol{H}}$ from the perspective of reconstructed 3D hearts, not simply from the magnitude of HSPs.

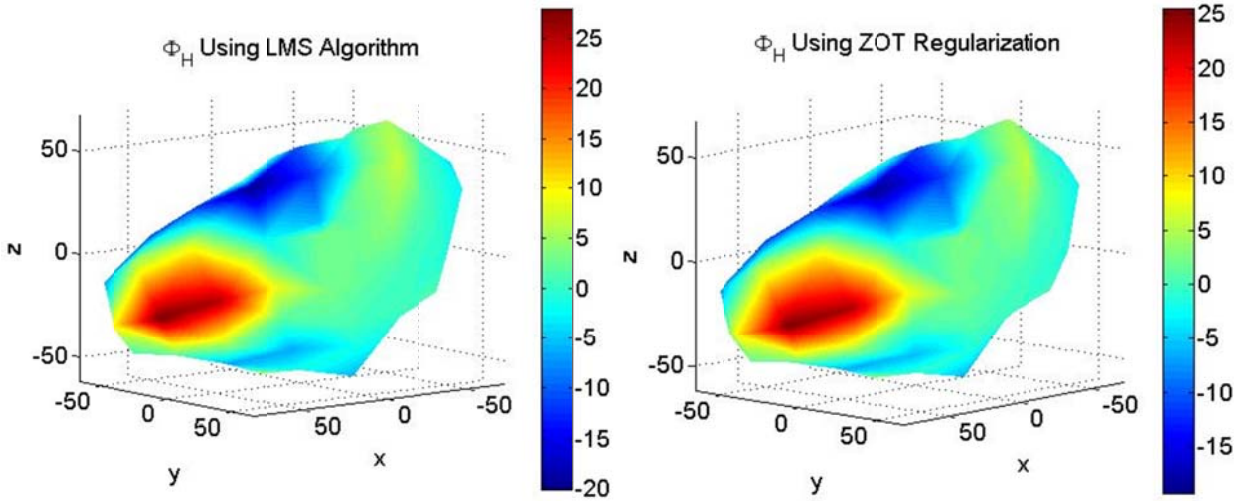

Fig. 11: Comparison of 3D HSPs generated from (Left) the LMS algorithm and (Right) the ZOT regularization.

From the above comparison, we see that the reconstructions of HSPs from the iterative LMS algorithm or the ZOT regularization are pretty close to each other. This result shows that the LMS algorithm can provide very similar spatial details of heart surface as the ZOT technique again, and this result also corresponds to the small relative error (RE) and high correlation coefficient (CC) between the estimate $\hat{\boldsymbol{\Phi}}_{\boldsymbol{H}}$ generated from the LMS iterative algorithm and the ZOT regularization, respectively. As for the L1-norm-based algorithm, the result is a little bit different.

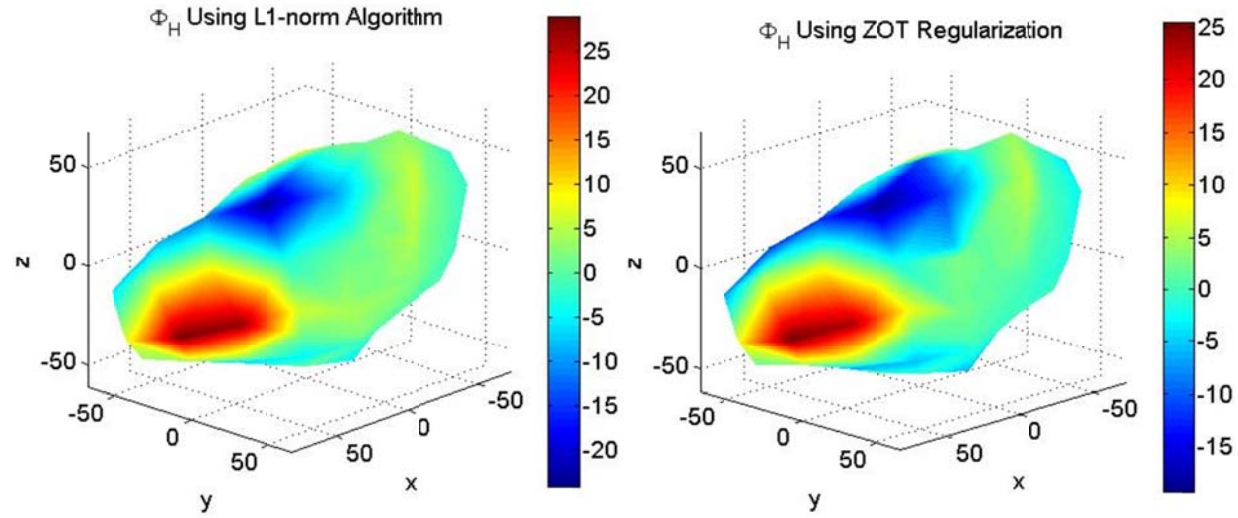

Fig. 12: Comparison of 3D HSPs generated from (Left) the L1-norm algorithm and (Right) the ZOT regularization.

Basically, the reconstruction of HSPs using the L1-norm-based regularization method is very close to the one generated by the ZOT regularization scheme. The only obvious difference appears in the T-wave region (the blue area at the top surface of the heart). The T-wave area shown in left heart, whose $\hat{\boldsymbol{\Phi}}_{\boldsymbol{H}}$ is generated from the L1-norm-based regularization, is a little smaller than the T-wave area in the ZOT heart, and this L1-norm heart is different from the LMS heart as well. Thus, the L1-norm heart may provide us with different spatial details of HSPs. Moreover, if we observe the color-bars in Fig.11 and Fig. 12, we can find that the range of the color-bars for the LMS heart and the L1-norm heart are both larger than the one of the ZOT heart. Among these three hearts, the L1-norm heart has the largest range of color-bar, which also shows that the L1-norm-based algorithm can give different spatial information regarding energy distribution on the heart surface.

We know there exists the following relationship between HSPs and BSPs:

$$\boldsymbol{\Phi}_{\boldsymbol{B}} = \boldsymbol{Z}_{\boldsymbol{BH}}\boldsymbol{\Phi}_{\boldsymbol{H}}. \qquad (24)$$

The transfer-coefficient matrix relating HSPs to BSPs, $\boldsymbol{Z}_{\boldsymbol{BH}}$, is known, and we have generated estimate HSPs $\hat{\boldsymbol{\Phi}}_{\boldsymbol{H}}$ from both the LMS algorithm and the L1-norm-based algorithm, so we can generate the estimate BSPs $\hat{\boldsymbol{\Phi}}_{\boldsymbol{B}}$ using Eq. (24) for the two iterative algorithms, respectively. The results for the LMS algorithm and the ZOT regularization are given below:

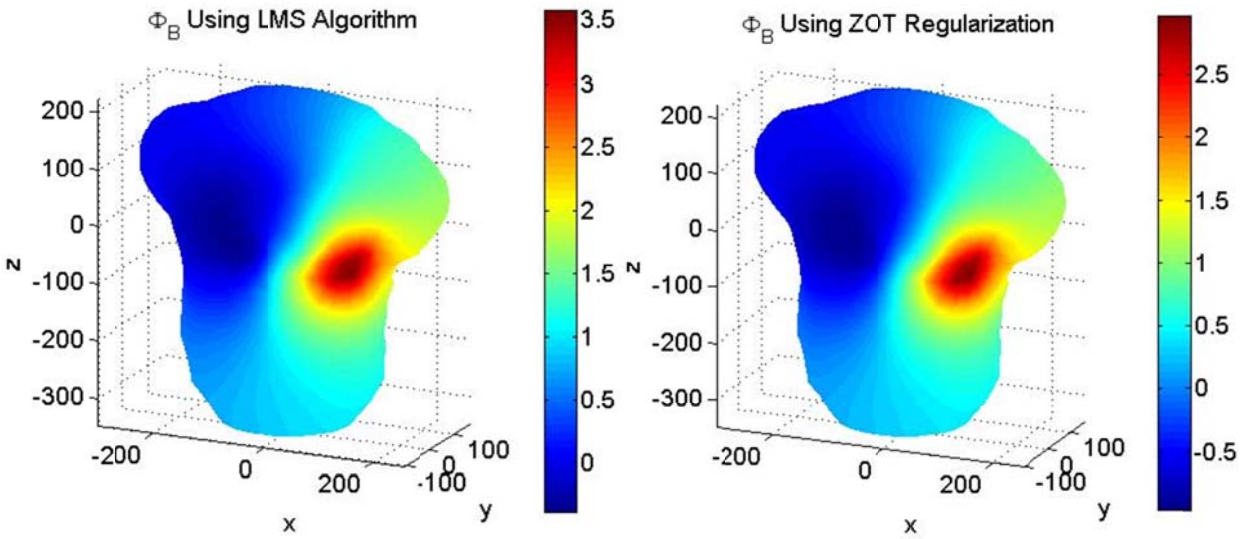

Fig. 13: Comparison of reconstructed BSPs generated from (Left) the LMS algorithm and (Right) the ZOT regularization.

Fig. 13 shows that not only the shapes of the reconstructed torso, but also the energy distributions on the body surface in the two plots are very close to each other. This is not a surprising simulation result, because $\hat{\boldsymbol{\Phi}}_{\boldsymbol{B}}$ is simply determined by $\hat{\boldsymbol{\Phi}}_{\boldsymbol{H}}$ in our assumption, and we have already shown that the $\hat{\boldsymbol{\Phi}}_{\boldsymbol{H}}$ generated from the LMS algorithm is a very good approximation to the $\hat{\boldsymbol{\Phi}}_{\boldsymbol{H}}$ generated from the ZOT

regularization. Thus, the corresponding BSPs $\hat{\boldsymbol{\Phi}}_{\boldsymbol{B}}$ should be close to each other as well. However, if we reconstruct the BSPs from the HSPs generated from the L1-norm-based iterative algorithm, we find that the reconstructed L1-norm torso is also very similar to the ZOT torso (Fig. 14).

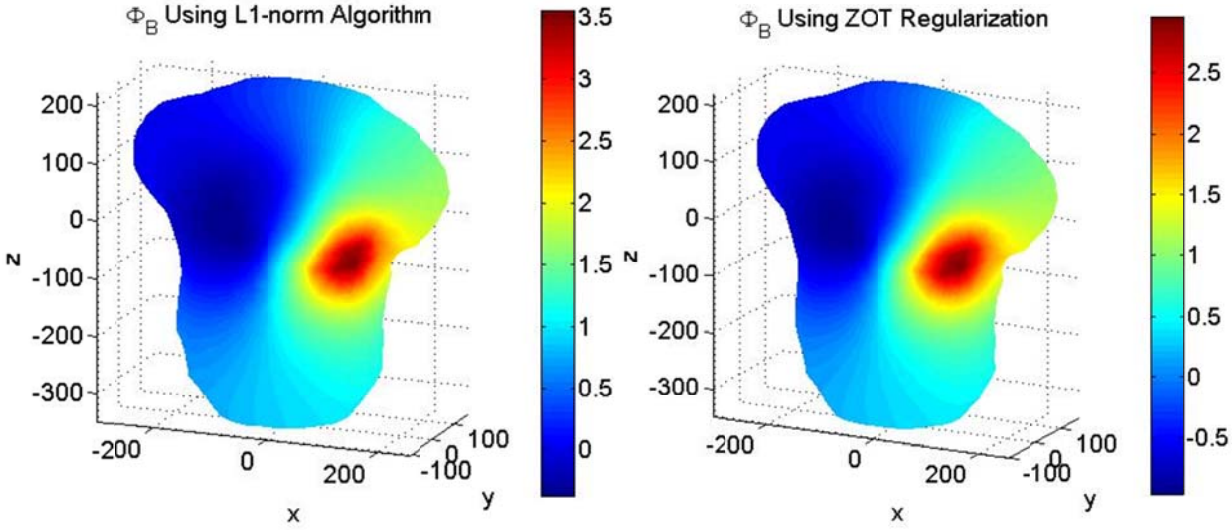

Fig. 14: Comparison of reconstructed BSPs generated from (Left) the L1-norm algorithm and (Right) the ZOT regularization.

Before we discuss the result generated from the L1-norm-based iterative regularization algorithm, let us look at the following the table first:

	LMS $\hat{\boldsymbol{\Phi}}_{\boldsymbol{B}}$ vs. ZOT $\hat{\boldsymbol{\Phi}}_{\boldsymbol{B}}$	L1-Norm $\hat{\boldsymbol{\Phi}}_{\boldsymbol{B}}$ vs. ZOT $\hat{\boldsymbol{\Phi}}_{\boldsymbol{B}}$
Relative error	**0.0540**	**0.0550**
Correlation coefficient	**0.9985**	**0.9985**

Table 3: Relative error and correlation coefficient between LMS/L1-norm $\hat{\boldsymbol{\Phi}}_{\boldsymbol{B}}$ and ZOT $\hat{\boldsymbol{\Phi}}_{\boldsymbol{B}}$.

Recall the data shown in Table 2, we obtain a smaller RE and a higher CC of $\hat{\boldsymbol{\Phi}}_{\boldsymbol{H}}$ from the iterative LMS algorithm than the L1-norm-based iterative regularization method. However, if we reconstruct the $\hat{\boldsymbol{\Phi}}_{\boldsymbol{B}}$ from the $\hat{\boldsymbol{\Phi}}_{\boldsymbol{H}}$, the RE and CC between LMS/ZOT and L1-norm/ZOT are almost the same. Hence, we can say that the reconstructed BSPs from the LMS algorithm and the L1-norm regularization method are both very close to the BSPs generated from the ZOT method. The LMS algorithm and the L1-norm-based regularization can provide us with very similar spatial details of the BSPs, even though the spatial details of HSPs given by the two algorithms are different.

IV. Discussion and Conclusion

In this project, we study and compare the algorithms of the ZOT regularization method, the iterative LMS technique, and the L1-norm-based iterative regularization scheme in detail. Generally, the

LMS iterative algorithm is simpler than both the ZOT regularization and the L1-norm-based iterative regularization, because the LMS algorithm does not involve computation of matrix inversions. Additionally, the parameter ε is simply based on the coefficient matrix $\boldsymbol{Z_{BH}}$ and the computation of eigenvalues, but we need to generate the L-curve to solve the regularization parameter λ for the L1-norm-based iterative regularization. However, compared with the LMS iterative algorithm, the L1-norm-based method takes much less iteration to achieve a local minimum solution $\widehat{\boldsymbol{\Phi}}_{\boldsymbol{H}}$.

As for the reconstructions of HSPs and BSPs generated from the ZOT regularization, the LMS algorithm, and the L1-norm-based method, respectively, we see that the ZOT regularization and the LMS algorithm can result in very close HSPs (RE = 0.1874 & CC = 0.9884). Thus, we could say the iterative LMS algorithm may be a good replacement for the ZOT regularization, since the ZOT regularization scheme needs to deal with the computations of matrix inversion and the regularization parameter. More importantly, the inverse solution provided by the ZOT regularization is sensitive to measurement errors, and the ZOT regularization cannot localize and distinguish multiple proximal cardiac electrical sources [3]. Using the LMS iterative algorithm instead can provide very similar spatial details while overcoming the inadequacies of the ZOT regularization scheme at the same time.

On the other hand, even though the estimate HSPs from the L1-norm-based regularization is not very close to the estimate HSPs from the ZOT regularization, we cannot say the L1-norm-based method is not a good regularization scheme. As what mentioned in the last paragraph, we know that there exist some inadequacies in solving the inverse ECG problems by using the ZOT regularization, so we cannot say the ZOT regularization is the most appropriate regularization technique for the inverse problem of ECG mappings. Hence, the difference between the estimate HSPs generated from the L1-norm-based regularization method and the ZOT regularization can provide us with some new spatial information, which may be very useful for the further studies of the depolarization and repolarization of action potential templates on HSPs. Similarly, the difference of the reconstructions of BSPs may also bring different spatial information for us.

Therefore, through this project, we discuss and compare different algorithms for solving the inverse problems of ECG mappings. We derive the iterative LMS algorithm, which could be a good equivalent algorithm for the ZOT regularization technique. Additionally, we develop the iterative L1-norm-based regularization algorithm, which may provide us with different spatial information of HSPs compared with the ZOT regularization technique and the LMS algorithm. Based on these different approaches to the ECG inverse problems, further clinical and bioengineering studies can be conducted to identify cardiac-associated risks.

V. Acknowledge

The author is grateful to Professor R. Martin Arthur of the Washington University in St. Louis for providing all the data used in this study.

VI. Reference

[1] R. Martin Arthur, **Yujing Lin**, Shuli Wang and Jason W. Trobaugh, "Effects of Changes in Action Potential Duration on the Electrocardiogram in Type II Diabetes," *International Journal of Bioelectromagnetism,* Vol. 14, No.3, December 2012.

[2] Guofa Shou, Ling Xia, and Mingfeng Jiang, "Total Variation Regularization in Electrocardiographic Mapping," *Life System Modeling and Intelligent Computing,* Vol. 6330, pp 51-59, 2010.

[3] Guofa Shou, Ling Xia, Feng Liu, Mingfeng Jiang and Stuart Crozier, "On Epicardial Potential Reconstruction Using Regularization Schemes with the L1-norm Data Term," *Physics in Medicine and Biology,* November 30, 2010.

[4] Daryl G. Beetner and R. Martin Arthur, "Estimation of Heart-Surface Potentials Using Regularized Multipole Sources," *Transactions on Biomedical Engineering, IEEE,* Vol. 51, No. 8, August 2004.

[5] Todd K. Moon and Wynn C. Stirling, "Mathematical Methods and Algorithms for Signal Processing," Ch. 14, pp 643 – 648, New Jersey, 2000. Print.

[6] Roger C. Barr, Maynard Ramsey. III, and Madison S. Spach, "Relating Epicardial to Body Surface Potential Distributions by Means of Transfer Coefficients Based on Geometry Measurements," *Transactions on Biomedical Engineering, IEEE,* Vol. BME-24, No. 1, January 1977.

[7] Lorange, M.; Gulrajani, R.M., "The forward and inverse problems of electrocardiography," *Engineering in Medicine and Biology Magazine, IEEE,* Vol. 17, No. 5, Sep/Oct 2008.

[8] Ghosh, Subham, "Electrocardiographic Imaging : Development of a Non-smooth Regularization Method and Clinical Application in Patients with Wolff-Parkinson-White Syndrome and Heart Failure," Ph.D. dissertation, Washington Univ., St. Louis, MO, 2009.

[9] Daryl G. Beetner, "Inference of Spectral and Temporal Characteristics of Pericardial Potentials Using Individualized Human Heart-Torso Models and the Multipole-Equivalent Method," Ph.D. dissertation, Washington Univ., St. Louis, MO, 1997.

[10] Per Christian Hansen, and Dianne Prost O'Leary, "The Use of the L-curve in the Regularization of Discrete Ill-posted Problems," Society for Industrial and Applied Mathematics, Vol. 14, No. 6, pp. 1487-1503, Nov. 1993.

VII. Appendices

- **Appendix A: Analysis on the Parameter ε of the Iterative LMS Algorithm [5]**

For optimizing a function, to minimize it – is to iterate in such a way that $f(x^{n+1}) < f(x^n)$. The general framework is to update x^n by

$$x^{n+1} = x^n + \alpha_n p_n, \quad (1)$$

where α_n is a scalar, denoting a step size, and p_n is a direction of motion, selected so that the successive steps decrease f.

We know that for a differentiable function $f: R^m \to R$ in some open set D, the gradient $\frac{\partial f}{\partial x}$ points in the direction of the maximum increase of f at the point x. Thus, Eq. (1) can be expressed as:

$$x^{n+1} = x^n - \alpha_n \nabla f(x^n), \quad (2)$$

the parameter α_n determines how far we move at step n. To simplify this algorithm, we usually use $\alpha_n = \alpha$ for some constant α.

To obtain the α, consider the following example:

$$f(x) = x^T R x - 2b^T x, \quad (3)$$

where R is symmetric positive definite and $x \in R^m$, and the initial value is x^0.

$$\nabla f(x) = 2Rx - 2b, \quad (4)$$

$$x^{n+1} = x^n - \alpha(2Rx - 2b) = x^n + 2\alpha(b - Rx^n). \quad (5)$$

Let x^* denote the solution to $Rx = b$. Shifting coordinates centered around x^*, and letting $\varepsilon = 2\alpha$, then we can rewrite Eq. (5) as:

$$x^{n+1} - x^* = x^n - x^* + \varepsilon(b - Rx^n), \quad (6)$$

Because x^* is the solution to $Rx = b$, $Rx^* = b$, so $Rx^* - b = 0$. Substituting $y^n = x^n - x^*$ and $Rx^* - b = 0$, we obtain:

$$y^{n+1} = y^n + \varepsilon(b - Rx^n + Rx^* - b) = y^n - \varepsilon R(x^n - x^*) = y^n - \varepsilon R y^n = (I - \varepsilon R)y^n, \quad (7)$$

$$\frac{y^{n+1}}{y^n} = (I - \varepsilon R), \quad (8)$$

$$\left(\frac{y^{n+1}}{y^n}\right)\left(\frac{y^n}{y^{n-1}}\right)\ldots\left(\frac{y^1}{y^0}\right) = (I - \varepsilon R)^{n+1}, \quad (9)$$

$$y^n = (I - \varepsilon R)^n y^0. \quad (10)$$

Convergence of this equation from any initial point $y^0 = x^0 + x^*$ requires that $\|I - \varepsilon R\| < 1$.

Let $\Lambda = QRQ^T$, where Q is the orthogonal matrix composed of eigenvectors of R, and Λ is the diagonal matrix of eigenvalues. Let $z = Qy$, then the Eq. (7) can be written as:

$$z^{n+1} = (QQ^T - \varepsilon QRQ^T)z^n, \quad (11)$$

which leads to the solution:

$$z^n = (I - \varepsilon\Lambda)^n z^0. \quad (12)$$

Since the matrix $I - \mu\Lambda$ is diagonal, Eq. (12) can be expressed as the set of decoupled equations:

$$z_1^n = (1 - \varepsilon\lambda_1)^n z_1^n,$$
$$z_2^n = (1 - \varepsilon\lambda_2)^n z_2^n,$$
$$\vdots$$
$$z_m^n = (1 - \varepsilon\lambda_m)^n z_m^n.$$

Therefore, it is clear that if we hope the convergence can occur from any starting point z^0, we must guarantee that:

$$|1 - \varepsilon\lambda_i| < 1, \quad i = 1,2, \dots, m.$$
$$0 < \varepsilon < \frac{2}{\lambda_i}, \quad i = 1,2, \dots, m.$$

Because a separateε is not provided for each direction, we must take the ε satisfying all constraints:

$$0 < \varepsilon < \frac{2}{\lambda_{max}}.$$

Now in our case, the objective function is:

$$J(\boldsymbol{h}) = (\boldsymbol{\Phi_B} - \boldsymbol{Z_{BH}}\boldsymbol{\Phi_H}[t])^2$$
$$= \boldsymbol{\Phi_B^T}\boldsymbol{\Phi_B} - \boldsymbol{\Phi_B^T}[t]\boldsymbol{Z_{BH}}\boldsymbol{\Phi_H}[t] - \boldsymbol{\Phi_H^T}\boldsymbol{Z_{BH}^T}\boldsymbol{\Phi_B} + \boldsymbol{\Phi_H^T}[t]\boldsymbol{Z_{BH}^T}\boldsymbol{Z_{BH}}\boldsymbol{\Phi_H}[t] \quad (13)$$

The gradient function is $\nabla J(\boldsymbol{h}) = -2\boldsymbol{\Phi_B^T}\boldsymbol{Z_{BH}} + 2\boldsymbol{Z_{BH}^T}\boldsymbol{Z_{BH}}\boldsymbol{\Phi_H}[t]$. Based on the proof shown above,

$$\boldsymbol{\Phi_H}[t+1] = \boldsymbol{\Phi_H}[t] + \varepsilon\big(\boldsymbol{\Phi_B^T}\boldsymbol{Z_{BH}} - \boldsymbol{Z_{BH}^T}\boldsymbol{Z_{BH}}\boldsymbol{\Phi_H}[t]\big), \quad (14)$$

Eq. (14) satisfies the form of Eq. (5), thus, the ε in Eq. (14) can also be obtained from:

$$0 < \varepsilon < \frac{2}{\lambda_{max}},$$

where λ_{max} is the maximum eigenvalue of R.

- **Appendix B: Analysis on the Normal Derivative Operator D for the L1-norm-based Iterative Regularization [9]**

  Green's second identity gives the following relationship:

$$\int_S (A\nabla B - B\nabla \mathrm{A}) \cdot \bar{n} dS = \int_V (A\nabla^2 B - B\nabla^2 \mathrm{A}) \cdot dV, \quad (1)$$

where *V* is the volume inside the surface *S*, $\bar{n}$ is an outward pointing vector of unit magnitude normal to surface element *dS*, and *A* and *B* are two scalar functions of position. By dividing either body surface ϕ_B or heart surface ϕ_H into inner and outer portions, and utilizing the fact that $\nabla\phi = 0$ on the outer surface, we can obtain the potential at point o described by [1]:

$$\phi^o = -\frac{1}{4\pi}\int_{S_H} \phi_H \frac{\bar{r}\cdot\bar{n}}{r^2} dS_H - \frac{1}{4\pi}\int_{S_H} \phi_H \frac{\nabla\phi_H\cdot\bar{n}}{r} dS_H + \frac{1}{4\pi}\int_{S_B} \phi_B \frac{\bar{r}\cdot\bar{n}}{r^2} dS_B, \quad (2)$$

where S_H and S_B are heart surface and body surface, respectively. Denote $\frac{\bar{r}\cdot\bar{n}}{r^2}dS_f = d\Omega_{ef}^i$, which means that subtended at an observation of the i[th] location on surface e by an area element on surface f. Specifically, choose two locations of observations, ϕ_B and ϕ_H, then (2) can be written as:

$$\phi_B^i = -\frac{1}{4\pi}\int_{S_H}\phi_H d\Omega_{BH}^i - \frac{1}{4\pi}\int_{S_H}\phi_H\frac{\nabla\phi_H\cdot\bar{n}}{r}dS_H + \frac{1}{4\pi}\int_{S_B}\phi_B d\Omega_{BB}^i, \qquad (3a)$$

$$\phi_H^i = -\frac{1}{4\pi}\int_{S_H}\phi_H d\Omega_{HH}^i - \frac{1}{4\pi}\int_{S_H}\phi_H\frac{\nabla\phi_H\cdot\bar{n}}{r}dS_H + \frac{1}{4\pi}\int_{S_B}\phi_B d\Omega_{HB}^i. \qquad (3b)$$

Assume that each of the terms in (3a) and (3b) can be discretized as:

$$-\phi_X^i + \frac{1}{4\pi}\int_{S_X}\phi_X d\Omega_{XX}^i = \sum_{j=1}^{N_X} p_{XX}^{ij}\phi_X^j, \qquad (4a)$$

$$-\frac{1}{4\pi}\int_{S_Y}\phi_Y d\Omega_{XY}^i = \sum_{j=1}^{N_Y} p_{XY}^{ij}\phi_X^j, \qquad (4b)$$

$$-\frac{1}{4\pi}\int_{S_Y}\phi_Y\frac{\nabla\phi_Y\cdot\bar{n}}{r}dS_H = \sum_{j=1}^{N_Y} g_{XY}^{ij}\Gamma_Y^j. \qquad (4c)$$

Substituting (4a)-(4c) into (3a) and (3b) gives:

$$p_{BB}^i\Phi_B + p_{BH}^i\Phi_H + g_{BH}^i\Gamma_H = 0, \qquad (5a)$$

$$p_{HB}^i\Phi_B + p_{HH}^i\Phi_H + g_{HH}^i\Gamma_H = 0. \qquad (5b)$$

By choosing the i[th] location successively at all N_B locations on surface S_B and then successively at all N_H locations on surface S_H as well, (5a) and (5b) can be written as:

$$P_{BB}\Phi_B + P_{BH}\Phi_H + G_{BH}\Gamma_H = 0, \qquad (5a)$$

$$P_{HB}\Phi_B + P_{HH}\Phi_H + G_{HH}\Gamma_H = 0, \qquad (5b)$$

where P's and G's are matrices of coefficients depending entirely on geometry. Γ_H can be obtained either from (5a) or (5b); however, G_{BH} is invertible and G_{BH} consists of coefficients of heart gradients as seen by an observer at body locations. Therefore, (5b) can provide a better Γ_H with less numerical error. From (5b), we can have:

$$\Gamma_H = -{G_{HH}}^{-1}(P_{HB}\Phi_B + P_{HH}\Phi_H). \qquad (6)$$

If only one surface is considered, for example, the heart-surface is taken into account, (5b) and (6) can be simplified as:

$$P_{HH}\Phi_H + G_{HH}\Gamma_H = 0, \qquad (7a)$$

$$\Gamma_H = -{G_{HH}}^{-1}P_{HH}\Phi_H. \qquad (7b)$$

Applying the above analysis to our problem, Γ_H exactly represents the operation:

$$\Gamma_H = \boldsymbol{D}\Phi_H = -{G_{HH}}^{-1}P_{HH}\Phi_H. \qquad (8)$$

Thus, the normal derivative operator $\boldsymbol{D} = -{G_{HH}}^{-1}P_{HH}$.

- **Appendix C: Matlab Code for the Iterative LMS Algorithm**

```
% Function: Using least-mean-square iterative algorithm to generate HSPs from BSPs.
% Variables:
% (1) zbheln:transfer-coefficient matrix relating HSPs to BSPs.
% (2) gecg: body-surface potentials
% (3) Ve_old/Ve_new: hear-surface potentials
% Input: iternum = iteration number
% Yujing Lin
% Washington University in St.Louis, ESE Dept.
% Apr.7,2013

function [logdiff1]=iteration_LMS(iternum)
load ar1018bip2;
Ve_old=zeros(80,1162);% initialization of Phi_H = 0
Ve_new=zeros(80,1162);
tic;
for k=1:1:iternum
    Ve_old=Ve_new;
    mu=1./(max(eig(zbheln'*zbheln)));      Ve_new=Ve_old+mu*(zbheln'*gecg'-zbheln'*zbheln*Ve_old);%
    use LMS iterative algorithm to generate new heart-surface potentials
    mean_std(k)=mean(std(Ve_new(:,(290:450))'));% used as a criterion to tell if iteration results
    converge
end
toc;

for m=1:1:(iternum-1)
    diffmeanstd(m)=mean_std(m+1)-mean_std(m);
end
logdiff1=log(diffmeanstd);

% plot and compare the estimate Phi_H and ppot
figure;subplot(211);plot(Ve_new');grid on;hold on;   set(gca,'FontSize',14);
plot(std(Ve_new),'c','LineWidth',2);
title(['\Phi_H at k = ' num2str(k),' Using LMS Algorithm']);
```

```
xlabel('n');ylabel('mV');
subplot(212);plot(ppot);grid on;hold on;set(gca,'FontSize',14);
plot(std(ppot'),'c','LineWidth',2);
title('\Phi_H Using ZOT Regularization');
xlabel('n');ylabel('mv');

figure;plot(Ve_new');grid on;hold on;set(gca,'FontSize',14);
plot(std(Ve_new),'c','LineWidth',2);
title(['\Phi_H at k = ' num2str(k),' Using LMS Algorithm']);
xlabel('n');ylabel('mV');
print -dmeta;
figure;plot(ppot);grid on;hold on;set(gca,'FontSize',14);
plot(std(ppot'),'c','LineWidth',2);
title('\Phi_H Using ZOT Regularization');
xlabel('n');ylabel('mv');
print -dmeta;

% plot mean(std(QRS))and log(diff(mean(std(QRS))))
figure;plot(mean_std,'LineWidth',2);grid on;set(gca,'FontSize',14);
title('\mu(\sigma(QRS))');
xlabel('Iteration Number');ylabel('\mu(\sigma(QRS))');
figure;plot(diffmeanstd,'LineWidth',2);grid on;set(gca,'FontSize',14);
title('\Delta(\mu(\sigma(QRS)))');
xlabel('Iteration Number');ylabel('\Delta(\mu(\sigma(QRS)))');
figure;plot(logdiff1,'LineWidth',2);grid on;set(gca,'FontSize',14);
title('log(\Delta(\mu(\sigma(QRS)))) between Each Iteration');
xlabel('Iteration Number');ylabel('log(\Delta(\mu(\sigma(QRS))))');

% calculate the relative error and correlation coefficient
[re1,cc1,act1,est1]=reccst(ppot,Ve_new');re1,cc1,

% plot 3-D heart based on estimate Phi_H
[ii,jj]=max(std(Ve_new));set(gca,'FontSize',14);
figure;trisurfv(inxhrt,ndfhrt,Ve_new(:,jj));set(gca,'FontSize',14);
```

```
title('\Phi_H Using LMS Algorithm');
xlabel('x');ylabel('y');zlabel('z');
shading interp;colorbar;
[ii,jj]=max(std(ppot'));
figure;trisurfv(inxhrt,ndfhrt,ppot(jj,:));set(gca,'FontSize',14);
title('\Phi_H Using ZOT Regularization');
xlabel('x');ylabel('y');zlabel('z');
shading interp;colorbar;
print -dmeta;
bsp=zbh*Ve_new; % calcuate body-surface-potential from estimate Phi_H
[mm,nn]=max(std(bsp));
bspe=zbheln*Ve_new;
[re2,cc2,act2,est2]=reccst(bspe,gecg');re2,cc2,
figure;trisurfv(inxtor,ndftor,bsp(:,nn));set(gca,'FontSize',14);
title('\Phi_B Using LMS Algorithm');
xlabel('x');ylabel('y');zlabel('z');
shading interp;
colorbar;
[mm,nn]=max(std(bspp'));
figure;trisurfv(inxtor,ndftor,bspp(nn,:));set(gca,'FontSize',14);
title('\Phi_B Using ZOT Regularization');
xlabel('x');ylabel('y');zlabel('z');
shading interp;
colorbar;
print -dmeta;

return
```

- **Appendix D: Matlab Code for the L1-norm-based Regularization Algorithm**

```
% Function: Using L1-norm-based iterative algorithm to generate HSPs from BSPs.
% Variables:
% (1) zbheln:transfer-coefficient matrix relating HSPs to BSPs.
% (2)gecg: body-surface potentials
% (3) phi_old/phi_new: hear-surface potentials
```

```
% Input: iternum = iteration number
% Yujing Lin
% Washington University in St.Louis, ESE Dept.
% Apr.7,2013

function [D,W,bsp]=iteration_L1(iternum)
load ar1018bip2;
tau_new=0.1836;
D=-inv(ghhn)*phhn; % differentiation operator D
phi_old=inv(zbheln'*zbheln+tau_new*D'*D)*zbheln'*gecg'; % initialization of estimate heart surface
potentials
phi_new=inv(zbheln'*zbheln+tau_new*D'*D)*zbheln'*gecg';
      beta=10^(-5);

% generate the weighting matrix W and the corresponding estimate Phi_H
for k=1:1:iternum
     phi_old=phi_new;
     D_phi=D*phi_old;
     L1_D=zeros(1,1162);
     for j=1:1:1162
          L1_D(1,j)=sum(abs(D_phi(:,j))); % take the absolute sum of each column of D
     end
     L1_D_L1norm=max(L1_D);% updating D*Phi_H
     W=diag(1/2./(sqrt((L1_D_L1norm)^2+beta))*ones(1,80));
     D_new=D'*W*D;
     phi_new=inv(zbheln'*zbheln+tau_new.*D_new)*zbheln'*gecg';
     mean_std(k)=mean(std(phi_new(:,(290:450))));
end

% calculate the difference of mean(std(QRS)) between each iteration
for m=1:1:(iternum-1)
     diffmeanstd(m)=mean_std(m+1)-mean_std(m);
end
```

```
% plot and compare the estimate Phi_H and ppot
figure;plot(phi_new');grid on;hold on;
set(gca,'FontSize',14);
plot(std(phi_new),'c','LineWidth',2);
title(['\Phi_H at k = ' num2str(k),' Using L1-norm Algorithm']);
xlabel('n');ylabel('mV');
print -dmeta;
figure;plot(ppot);grid on;hold on;set(gca,'FontSize',14);
plot(std(ppot'),'c','LineWidth',2);
title('\Phi_H Using ZOT Regularization');
xlabel('n');ylabel('mV');
print -dmeta;

% plot mean(std(QRS))
figure;plot(mean_std,'LineWidth',2);grid on;set(gca,'FontSize',14);
title('\mu(\sigma(QRS))');
xlabel('Iteration Number');ylabel('\mu(\sigma(QRS))');
print -dmeta;

% plot diff(mean(std(QRS)))
figure;plot(diffmeanstd,'LineWidth',2);grid on;set(gca,'FontSize',14);
title('\Delta(\mu(\sigma(QRS)))');
xlabel('Iteration Number');ylabel('\Delta(\mu(\sigma(QRS)))');
print -dmeta;

figure;plot(20*log10(abs(diffmeanstd)),'LineWidth',2);
set(gca,'FontSize',14);grid on;
xlabel('Iteration Number'); ylabel('dB');
title('log|\Delta(\mu[std(QRS)])|');
print -dmeta;

% calculate the relative error and correlation coefficient
[re1,cc1,act1,est1]=reccst(ppot,phi_new');re1,cc1,
```

```
% plot 3-D heart based on estimate Phi_H
[ii,jj]=max(std(phi_new));
figure;trisurfv(inxhrt,ndfhrt,phi_new(:,jj));set(gca,'FontSize',14);
title('\Phi_H Using L1-norm Algorithm');
xlabel('x');ylabel('y');zlabel('z');
shading interp;colorbar;
[ii,jj]=max(std(ppot'));
figure;trisurfv(inxhrt,ndfhrt,ppot(jj,:));set(gca,'FontSize',14);
title('\Phi_H Using ZOT Regularization');
xlabel('x');ylabel('y');zlabel('z');
shading interp;colorbar;
print -dmeta;
bsp=zbh*phi_new; % calcuate body-surface-potential from estimate Phi_H
[mm,nn]=max(std(bsp));
bspe=zbheln*phi_new;
[re2,cc2,act2,est2]=reccst(bspe,gecg');re2,cc2,
figure;trisurfv(inxtor,ndftor,bsp(:,nn));set(gca,'FontSize',14);
title('\Phi_B Using L1-norm Algorithm');
xlabel('x');ylabel('y');zlabel('z');
shading interp;
colorbar;
[mm,nn]=max(std(bspp'));
figure;trisurfv(inxtor,ndftor,bspp(nn,:));set(gca,'FontSize',14);
title('\Phi_B Using ZOT Regularization');
xlabel('x');ylabel('y');zlabel('z');
shading interp;
colorbar;
print -dmeta;

return;
```